Electronic Supplementary Material (ESI) for New Journal of Chemistry.

Supplementary Information for

Molecular level insight into the direct health impacts of some organic aerosol components

Fatemeh Keshavarz*

Institute for Atmospheric and Earth System Research, Faculty of Science, University of Helsinki, FI-00014 Helsinki, Finland

Department of Physics, School of Engineering Science, LUT University, FI-53851 Lappeenranta, Finland

* Corresponding author: Fatemeh Keshavarz: fatemeh.keshavarz@helsinki.fi, fatemeh.keshavarz@lut.fi, keshavarz.f.s@gmail.com

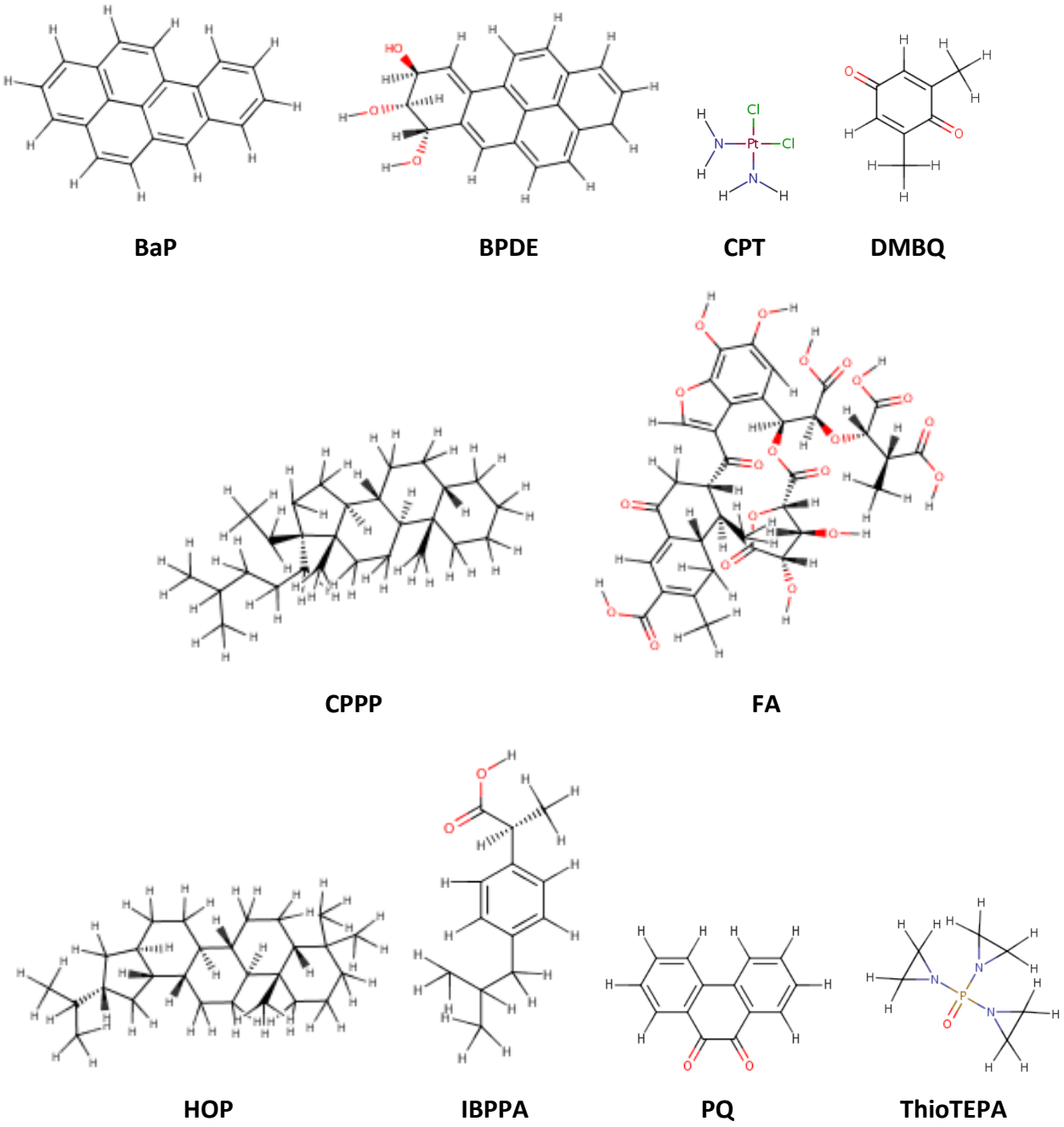

Fig. S1 2D structures of the model OA (FA), PQ, DMBQ, BaP, BPDE, HOP, CPPP, CPT, thioTEPA and IBPPA.

Table S1 Summary of the HSA docking results*

Ligand	Interaction energy	Electrostatic interaction	Hydrogen bonding	LE	Binding site
BaP	-115.3	0.0	0.0	-5.52	Arg 144* (-30.4), Arg 185, Gly 188, Ile 141, Lys 189, Phe 156
BPDE	-127.0	0.0	-6.4	-5.77	Arg 144, Arg 185, Asp 107, Gly 188, Ile 141, Lys 189* (-20.1), Phe 156
CPPP	-116.3	0.0	0.0	-4.31	Arg 185, Arg 427, Asp 186, Glu 424* (-21.9), Ile 522, Lys 189
CPT	-45.9	0.0	-8.0	-9.17	Lys 189* (-7.0)
DMBQ	-79.1	0.0	-2.5	-7.91	Arg 144, Gly 188, Ile 141* (-12.9), Lys 189, Phe 156
FA	-230.3	0.0	-14.7	-4.19	Arg 144, Arg 185* (-43.6), Asp 107, Asp 182, Glu 519, Gly 188, Ile 141, Lys 189, Phe 156
HOP	-109.7	0.0	0.0	-4.06	Arg 144, Arg 185* (-39.9), Lys 189
IBPPA	-99.1	0.0	-5.0	-6.61	Arg 144, Arg 185* (-18.6), Asp 107, Gly 188, Ile 141, Leu 184, Lys189, Phe 156, Tyr 160
PQ	-119.9	0.0	0.0	-7.49	Arg 185, Gly 188, Ile 141, Lys 189, Phe 148, Phe 156* (-17.8)
ThioTEPA	-79.7	0.0	0.0	-7.25	Arg 144, Arg 185, Gly 188, Ile 141* (-14.5), Lys 189, Phe 156

* The energy and ligand efficiency (LE=Interaction energy/number of non-hydrogen atoms) values are unitless. For binding site residues, the energy threshold of -7.0 is considered and the residue with the best (lowest) interaction energy is indicated by an asterisk and the corresponding total interaction energy value is reported in parenthesis.

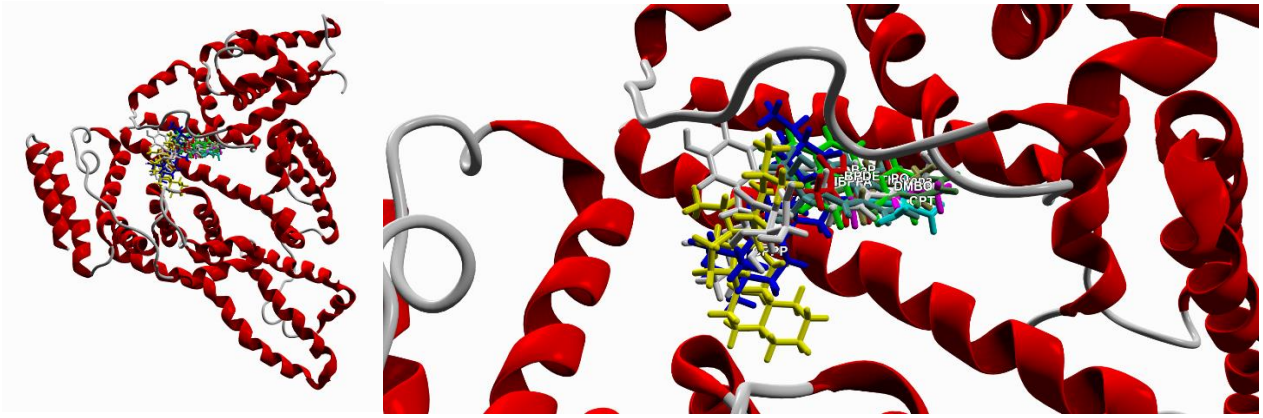

Fig. S2 HSA-ligand binding modes (Left: the general view, and right: the close up view with ligand names).

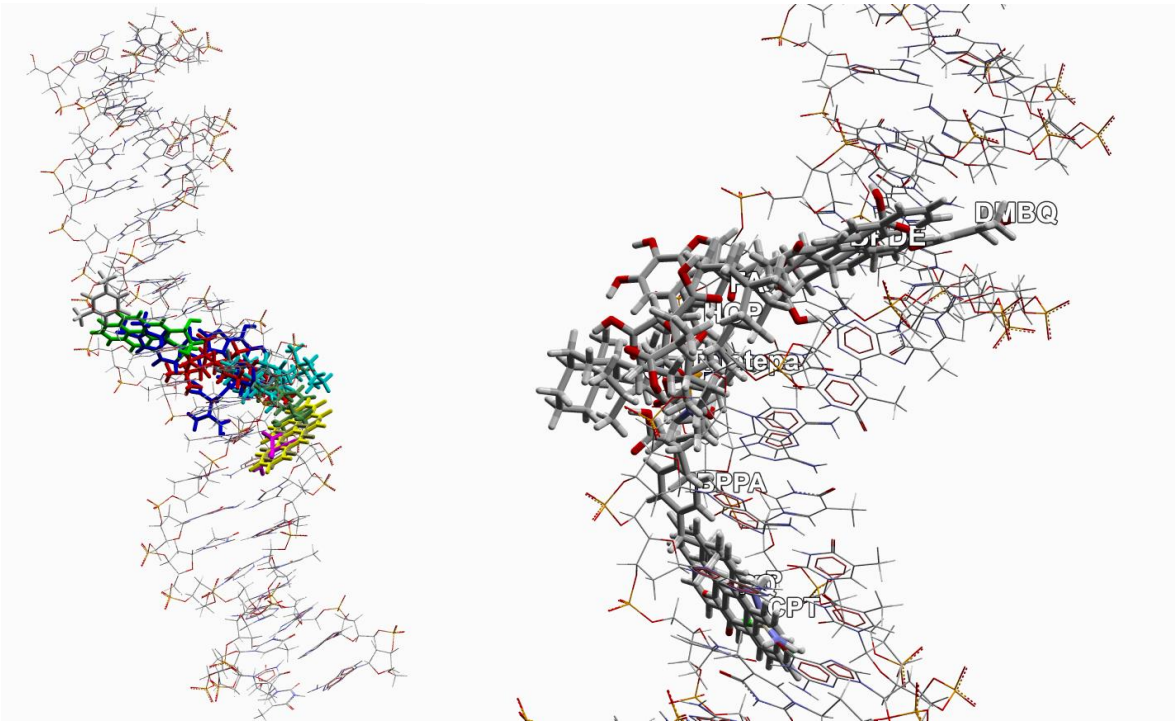

Fig. S3 3US0-ligand binding modes (Left: the general view, and right: the close up view with ligand names).

Table S2 Summary of the 4AWL docking results*

Ligand	Interaction energy	Electrostatic interaction	Hydrogen bonding	LE	Binding site
BaP	-131.5	0.0	0.0	-6.72	TGA/ACT
BPDE	-154.5	0.0	0.0	-6.57	TGA/ACT
CPPP	-112.8	0.0	0.0	-4.18	GTG/CAC
CPT	-51.6	0.0	0.0	-10.31	TG/AC
DMBQ	-77.9	0.0	0.0	-7.79	TGA/ACT
FA	-186.9	0.0	0.0	-3.40	CGGT/GCCA
HOP	-107.9	0.0	0.0	-3.99	TCG/AGC
IBPPA	-114.4	0.0	0.0	-7.63	CCA/GGT
PQ	-109.5	0.0	0.0	-6.85	CAC/GTG
ThioTEPA	-70.8	0.0	0.0	-6.44	AC/TG

* The energy and ligand efficiency (LE=Interaction energy/number of non-hydrogen atoms) values are unitless.

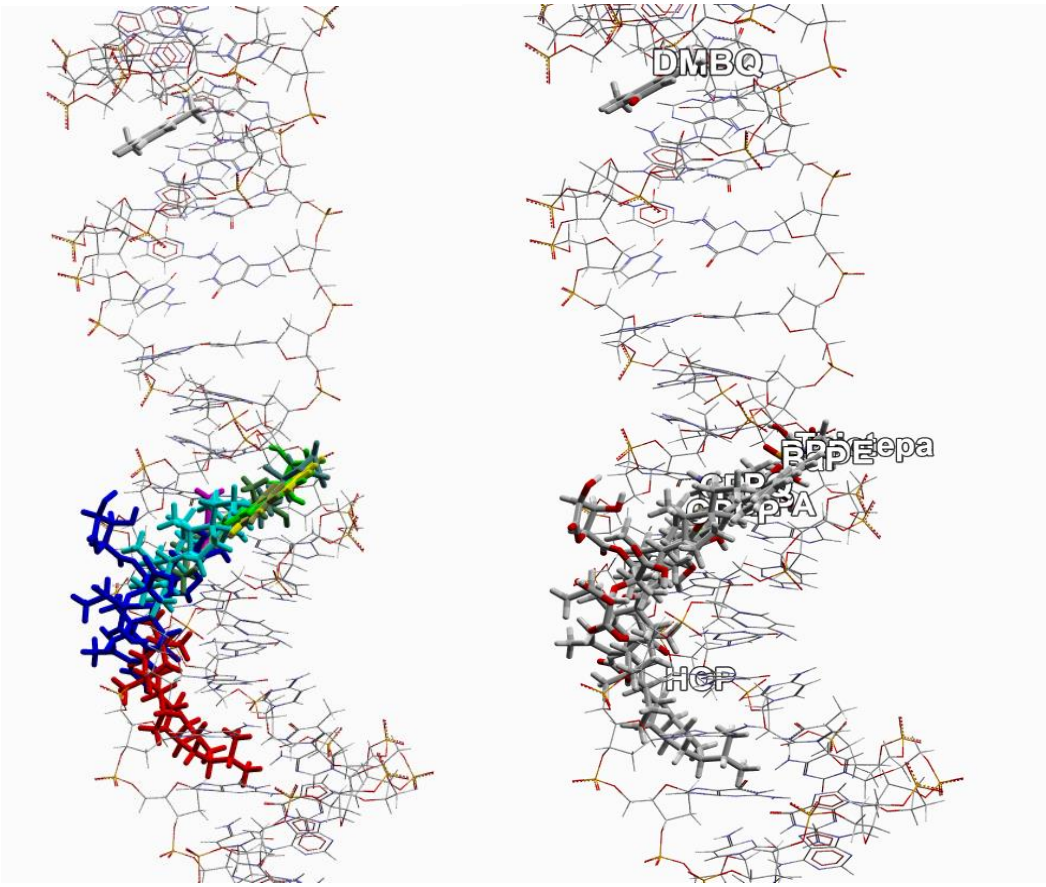

Fig. S4 4AWL-ligand binding modes (Left: the general view, and right: the close up view with ligand names).

Table S3 Second-order perturbation energies ($E^{(2)}$ stabilization energy; kJ mol^{-1}) associated with charge transfer from (donor)/to (acceptor) NBOs of the ligand-3US0 complexes in the form of NBO type(atom/bond$_{unit}$)$_{ligand\ or\ nucleotide}$ *

From	To	$E^{(2)}$	From	To	$E^{(2)}$
BaP			DMBQ		
LP*(C)$_{BaP}$	σ*(CH$_{dR}$)$_{nA}$	9.7	σ(CH)$_{DMBQ}$	σ*(CH$_{A}$)$_{nA}$	12.0
σ(CH)$_{BaP}$	σ*(CH$_{A}$)$_{nA}$	35.2	σ(CH$_{A}$)$_{nA}$	σ*(CH)$_{DMBQ}$	16.9
σ(CH)$_{BaP}$	σ*(CH$_{C}$)$_{nC}$	12.2	σ(CH$_{dR}$)$_{nT}$	σ*(CH)$_{DMBQ}$	15.4
σ(CH)$_{BaP}$	σ*(NC$_{A}$)$_{nA}$	10.1	IBPPA		
σ(CH$_{dR}$)$_{nA}$	LP*(C)$_{BaP}$	14.5	σ(CH)$_{IBPPA}$	σ*(CH$_{dR}$)$_{nT}$	26.8
LP(O$_{T}$)$_{nT}$	σ*(CC)$_{BaP}$	9.0	LP*(C)$_{IBPPA}$	σ*(CH$_{dR}$)$_{nA}$	10.7
σ(CH$_{C}$)$_{nC}$	σ*(CH)$_{BaP}$	15.9	σ(CH)$_{IBPPA}$	σ*(CH$_{dR}$)$_{nC}$	10.3
σ(CH$_{A}$)$_{nA}$	σ*(CH)$_{BaP}$	34.0	σ(CH)$_{IBPPA}$	σ*(CH$_{dR}$)$_{nA}$	20.8
σ(CH$_{A}$)$_{nA}$	σ*(CH)$_{BaP}$	15.7	σ(CH$_{dR}$)$_{nC}$	σ*(CH)$_{IBPPA}$	16.6
σ(CN$_{A}$)$_{nA}$	σ*(CH)$_{BaP}$	8.8	σ(CH$_{dR}$)$_{nA}$	LP(C)$_{IBPPA}$	13.1
LP(N$_{A}$)$_{nA}$	σ*(CC)$_{BaP}$	24.5	σ(CH$_{dR}$)$_{nA}$	σ*(CH)$_{IBPPA}$	16.0
BPDE			σ(CH$_{dR}$)$_{nC}$	σ*(CH)$_{IBPPA}$	12.5
σ(OH)$_{BPDE}$	σ*(CH$_{dR}$)$_{nA}$	50.1	PQ		
LP(O)$_{BPDE}$	σ*(CH$_{dR}$)$_{nA}$	14.7	LP(C)$_{PQ}$	σ*(CH$_{dR}$)$_{nT}$	10.3
LP(O)$_{BPDE}$	σ*(CH$_{dR}$)$_{nA}$	85.9	σ(CH)$_{PQ}$	σ*(CH$_{A}$)$_{nA}$	18.5
σ(CH)$_{BPDE}$	σ*(CH$_{A}$)$_{nA}$	11.1	σ(CH$_{dR}$)$_{nT}$	LP(C)$_{PQ}$	8.7
σ(OH)$_{BPDE}$	σ*(CH$_{A}$)$_{nA}$	57.2	σ(CH$_{A}$)$_{nA}$	σ*(CH)$_{PQ}$	35.0
σ(OH)$_{BPDE}$	σ*(CN$_{A}$)$_{nA}$	11.5	LP(N$_{A}$)$_{nA}$	LP*(C)$_{PQ}$	13.3
LP(O)$_{BPDE}$	σ*(CH$_{dR}$)$_{nT}$	9.5	LP(N$_{A}$)$_{nA}$	σ*(CH)$_{PQ}$	13.7
LP(O)$_{BPDE}$	σ*(CH$_{dR}$)$_{nT}$	11.4			
LP(O)$_{BPDE}$	σ*(CH$_{A}$)$_{nA}$	40.8			
LP(O)$_{BPDE}$	σ*(CH$_{dR}$)$_{nT}$	12.2			
σ(OC$_{dR}$)$_{nA}$	σ*(OH)$_{BPDE}$	19.2			
σ(CH$_{dR}$)$_{nA}$	σ*(OH)$_{BPDE}$	82.1			
LP(O$_{dR}$)$_{nA}$	σ*(OH)$_{BPDE}$	58.8			
LP(N$_{A}$)$_{nA}$	σ*(CH)$_{BPDE}$	38.8			
σ(CH$_{A}$)$_{nA}$	σ*(OH)$_{BPDE}$	181.1			
σ(CN$_{A}$)$_{nA}$	σ*(OH)$_{BPDE}$	19.4			

* The energy threshold of 8.2 kJ mol^{-1} (= 2 kcal mol^{-1}) is considered. For 3US0, the nucleotide (nA, nC, nT and nG) units include the deoxyribose of the DNA backbone (dR) and the nucleobases (A, T, C or G). No significant charge transfer was observed between the phosphate backbone (PO4) and the ligands.

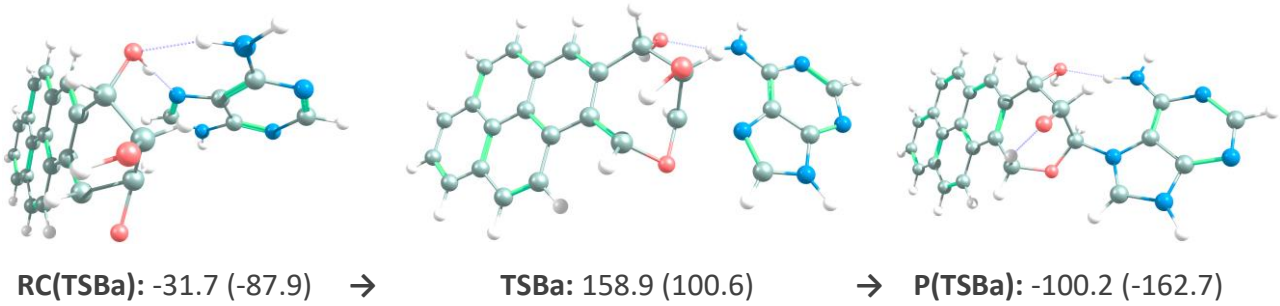

Fig. S5 The mechanism of adduct formation between the A nucleobase and BPDE at the ωB97X-D/3-21g level of theory. The Gibbs free energies (and ZPE-corrected energy values) are reported in kJ mol^{-1} relative to the reactants. The carbon, hydrogen, oxygen, and nitrogen atoms are represented as grey, white, red, and blue balls, respectively.

Steps II & IV: Protonation by H^+

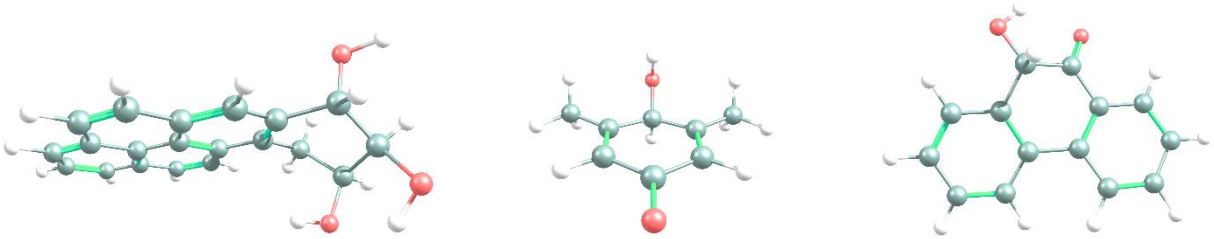

BPDEh$^-$ → BPDEp: -669.6 (-695.4) DMBQh$^-$ →DMBQp: -675.1 (-702.0) PQh$^-$ → PQp: -672.6 (-698.3)

DMBQph$^-$ →DMBQpp: -694.5 (-720.3) PQph$^-$ → PQpp: -674.3 (-700.8)

Fig. S6 The protonated structures of the organic aerosol components from steps II and IV of the oxidative stress mechanism, along with the protonation Gibbs free energies (and ZPE-corrected energy values) in kJ mol^{-1}. The carbon, hydrogen, oxygen, and nitrogen atoms are represented as grey, white, red, and blue balls, respectively.

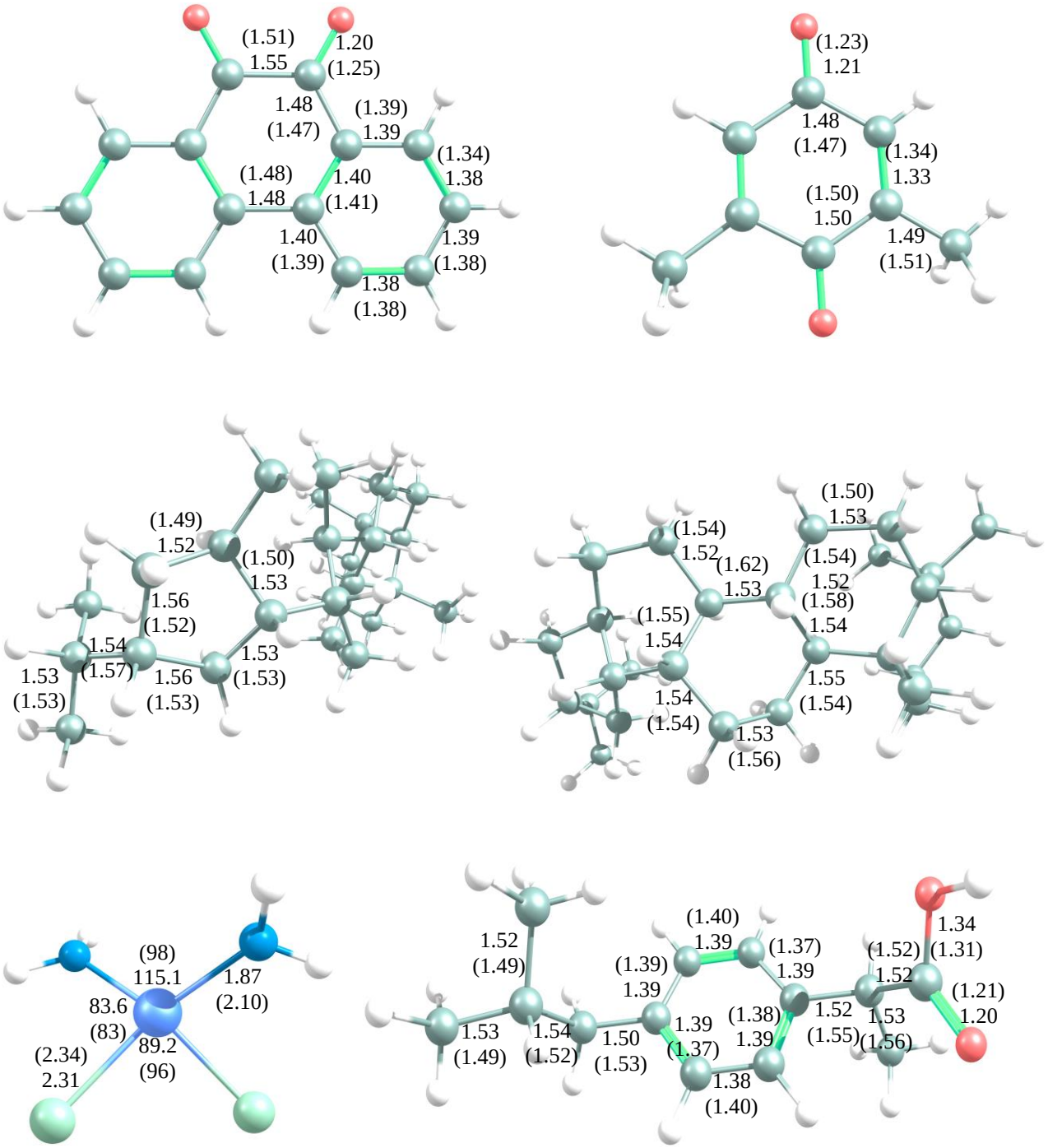

Fig. S7 Comparison of the structural parameters of the geometries optimized at the ωB97X-D/def2-TZVP level of theory (gas-phase) with the available experimental data. The bond lengths and bond angles are respectively reported in Å and °. The values in parenthesis refer to the experimentally determined crystals of the fully symmetric A form of 9, 10-phenanthrenequinone (PQ),[1] 2, 5-dimethyl-1, 4-benzoquinone (DMBQ),[2] 29-nor-17αH-hopane (HOP),[3] cis-platin (CPT),[4] and (S)-(+)-ibuprofen (IBPPA)[5]. The carbon, hydrogen, oxygen, nitrogen, chloride and platinum atoms are represented as grey, white, red, blue, light green and light purple balls, respectively.

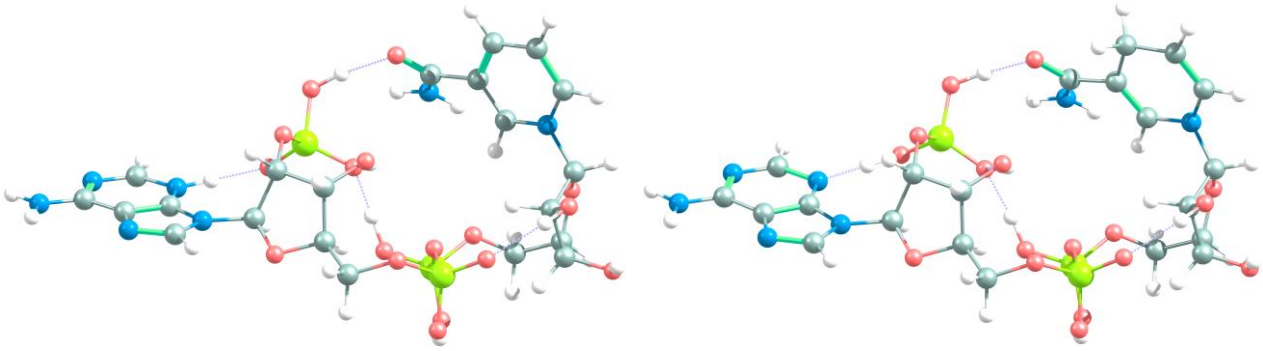

Fig. S8 Structure of the most stable conformer of $NADP^+$ (left) and NADPH (right) optimized at the ωB97X-D/def2-TZVP level of theory in water solvent. The carbon, hydrogen, oxygen, nitrogen, and phosphor atoms are represented as grey, white, red, blue, and phosphorous balls, respectively.

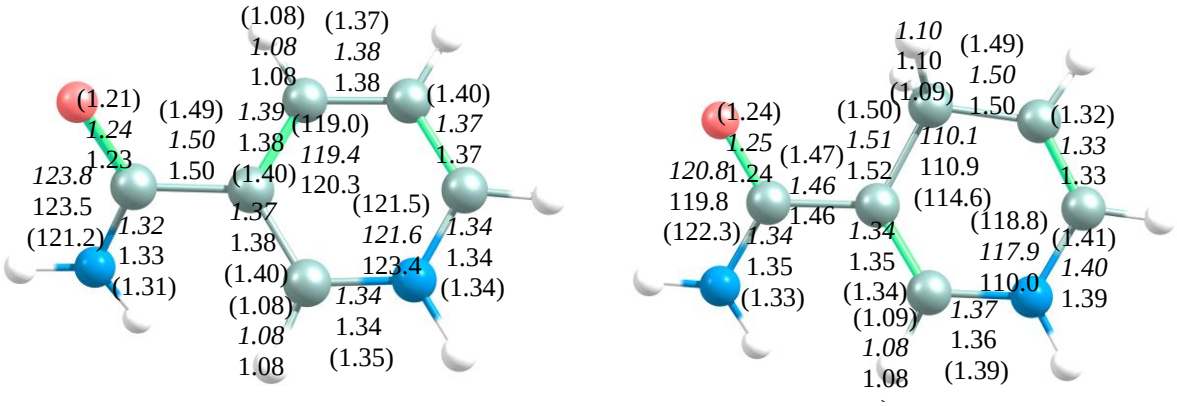

Fig. S9 Comparison of the structural parameters of the $NADP^+$ (left) and NADPH (right) models optimized at the ωB97X-D/def2-TZVP level of theory in solvent with the parameters related to the complete NADP+ and NADPH geometries optimized at the same level of theory (in *italic*) and the experimental data retrieved from XRD crystal structures with the Protein Data Bank (PDB) codes of 5OOG for $NADP^+$ [6] and 5W3Q[7] for NADPH (in parenthesis). The bond lengths and bond angles are respectively reported in Å and °. The carbon, hydrogen, oxygen and nitrogen atoms are represented as grey, white, red and blue balls, respectively.

References

(1) S. Y. Matsuzaki, M. Gotoh and A. Kuboyama, Molecular and Crystal Structure of the α and β Forms of 9, 10-Phenanthrenequinone, *Mol. Cryst. Liq. Cryst.*, 1987, **142**, 127-139.

(2) D. Rabinovich and G. M. J. Schmidt, Topochemistry. Part V. The crystal Structure of 2, 5-Dimethyl-1, 4-Benzoquinone, *J. Chem. Soc. (Resumed)*, 1964, 2030-2040.

(3) G. W. Smith, The Crystal and Molecular Structure of 29-nor-17αH-Hopane, $C_{29}H_{50}$, *Acta Crystallog. B*, 1975, **31**, 526-530.

(4) P. Carloni, M. Sprik and W. Andreoni, Key Steps of the Cis-Platin-DNA Interaction: Density Functional Theory-Based Molecular Dynamics Simulations, *J. Phys. Chem. B*, 2000, **104**, 823-835.

(5) A. A. Freer, J. M. Bunyan, N. Shankland and D. B. Sheen, Structure of (S)-(+)-Ibuprofen, *Acta Crystallog. C*, 1993, **49**, 1378-1380.

(6) N. M. Nesbitt, X. Zheng, Z. Li, J. A. Manso, W. Y. Yen, L. E. Malone, J. Ripoll-Rozada, P. J. B. Pereira, T. J. Mantle, J. Wang and W. F. Bahou, In Silico and Crystallographic Studies Identify Key Structural Features of Biliverdin IXβ Reductase Inhibitors Having Nanomolar Potency, *J. Biol. Chem.* 2018, **293**, 5431-5446.

(7) D. Oyen, R. B. Fenwick, P. C. Aoto, R. L. Stanfield, I. A. Wilson, H. J. Dyson and P. E. Wright, Defining the Structural Basis for Allosteric Product Release from E. coli Dihydrofolate Reductase using NMR Relaxation Dispersion, *J. Am. Chem. Soc.*, 2017, **139**, 11233-11240.